Identification of the Temporal Source of Frequency Domain Characteristics of SiC MOSFET Based Power Converter Waveforms

Sam Walder, Xibo Yuan, Ian Laird, Jeremy Dalton

Abstract—**Certain Electromagnetic Interference (EMI) performance characteristics that occur in data taken from practical systems are often difficult to attribute to time domain features as waveforms will tend to deviate from the idealized analytical case. This paper shows that by taking multiple derivatives of experimental data and comparing this with the expected characteristics of a typical switching waveform it is possible to understand exactly which features of a given temporal waveform lead to certain spectral characteristics. It is also shown through analysis of analytical methods and experimental data that the smoother the transitions of a waveform the faster the roll off of the spectral content and hence the better the EMI performance.**

Index Terms—**Silicon Carbide, Spectral Analysis, EMI**

I. INTRODUCTION

In modern power electronics it is still common to analyze the waveforms observed (both for current and voltage) at the switching nodes in terms of the classical trapezoidal waveform illustrated in Figure 1, the frequency domain envelope of which is easily calculated and widely reported [1]–[3]. However, as switching speeds and frequencies increase with the use of wide-bandgap technologies such as Silicon Carbide (SiC), the use of more detailed and accurate modeling techniques becomes necessary to account for the increases in slew-rate, overshoot and ringing.

When considering experimental data it can be found that the frequency domain characteristics do not conform to those predicted by basic modeling techniques. This is a problem for high performance converters as it is common to need to comply with EMI limits and being able to accurately predict the EMI before building a converter is critical.

The switching nodes of the converter (before any output filtering) are typically where noise originates as there are high speed switching edges of large amplitudes. Most of the waveforms' frequency spectrum envelope for low frequencies ($< 10\ MHz$) will be defined by the shape of the PWM waveform. Other aspects, such as the waveforms smoothness, ringing and overshoot will dictate the high frequency performance.

This paper will show that through the use of higher order models such as those discussed in [2], [4]–[6], it is possible to identify the time domain source of more complicated frequency domain characteristics than is possible with the trapezoidal model alone. An example SiC MOSFET based converter is considered and the relation of the losses and EMI performance investigated.
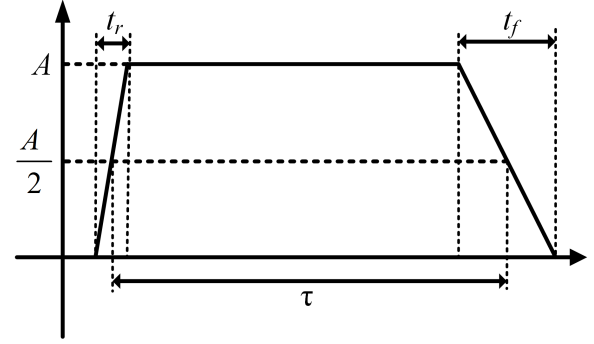

Fig. 1. Illustration of the trapezoidal approximation of a typical power electronics waveforms with defining parameters. A - Amplitude, τ - On period, t_r - Rise time, t_f - Fall time.

II. ALTERNATIVE ANALYSIS TECHNIQUES

The deviation of an experimental waveform from the shape it is approximated by for a given analytical method will lead to differences in the frequency domain. These differences will often be at high frequencies as the more subtle temporal characteristics tend to have high frequency break points. These differences can cause the roll off at higher frequencies to be higher than predicted by traditional models which will be beneficial where EMI performance is a concern. Typically the trapezoidal approximation will not be sufficient to model these high frequency effects and a more advanced model has to be used if the performance is to be predicted accurately.

Other works have identified a number of other methods by which the switching waveforms observed can be modeled besides the trapezoidal method. [6] demonstrates an 'S' shaped waveform which extends the roll off of the spectral components of the signal to 60 dB/dec at higher frequencies. This work also demonstrates that the idealized switching waveform would not cause any further switching losses.

The smoother the waveform shape the faster the expansion coefficients of the Fourier transform roll off. As smoothness is defined as the number of times a waveform can be differentiated before a non-continuous function results, introducing further derivatives will improve the EMI performance of the system [7]. At the limit a perfectly smooth (infinitely differentiable) waveform can be used which will mean that the roll off of spectral components will increase exponentially with frequency.

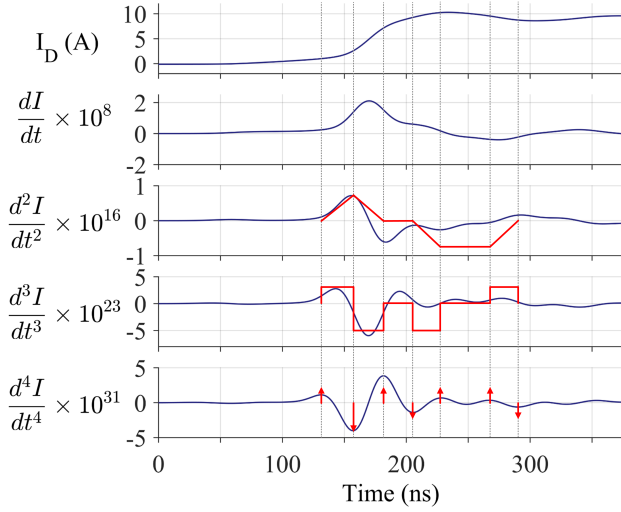To illustrate how the rate of roll-off of the Fourier coef-

Fig. 2. Illustration of square, trapezoidal, 'S' shaped and 4th derivative controlled waveforms and their derivatives.

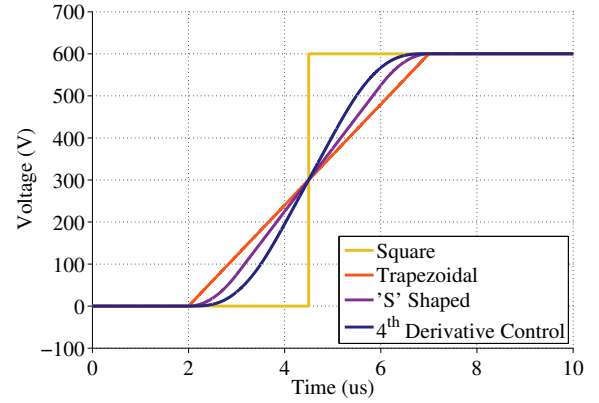| Symbol	Definition
A	Amplitude of the root waveform
T	Period
τ	On period
n	Harmonic number
ω_0	Angular frequency of the waveform
τ_r	Rise-time of trapezoidal waveform
τ_f	Fall-time of trapezoidal waveform
$\tau_{r(dV/dt)}$	Rise time of the first derivative

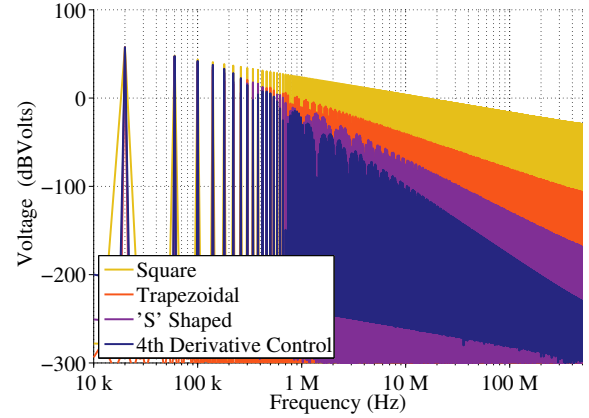Fig. 3. Comparison of the typical shape of waveforms with various levels of smoothing.

Fig. 4. Comparison of the spectral content of waveforms with differing levels of smoothness.

ficients increases with increasing smoothness the concept of the 'S' shaped waveform can be extended to create smoother waveforms to analyze. Figure 2 illustrates four waveforms, starting with the basic square wave and becoming progressively smother with each additional derivation before the Dirac functions are encountered. By considering the derivatives of the functions presented it is possible to derive an expression for the Fourier series coefficients for each of these waveforms [8]. The expressions for the first three cases are given in Equations (1) to (4) with the symbols used defined in Table I.

Square waveform expansion coefficients:

$$c_n = \frac{A}{2} sinc(\frac{n\pi}{2}) \tag{1}$$

Triangular waveform expansion coefficients:

$$c_n = A\frac{\tau}{T} sinc(n\omega_0 \frac{\tau}{2}) sinc(n\omega_0 \frac{\tau_r}{2}) e^{-jn\omega_0 \frac{\tau+\tau_r}{2}} \tag{2}$$

For the 'S' shaped waveform [9]:

$$c_n = A\frac{\tau}{T} sinc(n\omega_0 \frac{\tau}{2}) sinc(n\omega_0 \frac{\tau_r - \tau_{r(dV/dt)}}{2}) \times \\ sinc(n\omega_0 \frac{\tau_{r(dV/dt)}}{2}) e^{-jn\omega_0 \frac{\tau+\tau_r}{2}} \tag{3}$$

For all of the above:

$$sinc(x) = \frac{sin(x)}{x} \tag{4}$$

A notable feature of these equations is that with each additional derivative introduced before Dirac functions are observed an additional $sinc()$ function is introduced to the expression for the Fourier expansion coefficients. Each of these contributes a -20 dB/dec roll off to the envelope of the spectrum after its particular break-point. The maximum roll off for a waveform that can be differentiated P times will hence be $-20P\ dB/dec$. Figures 3 and 4 show the comparison of some idealized waveforms of increasing smoothness and the Discrete Fourier Transform (DFT) of these waveforms. The maximum roll off predicted by the expressions shown here is clearly visible on the envelope of the spectra shown in Figure 4. Both Figure 4 and the equations presented demonstrate that the higher the degree of smoothness the greater the improvements in EMI performance will be.

At the limit a waveform can be completely smooth, that is, it is infinitely differentiable. Works such as [2] have investigated smoother waveforms than the basic case and works such as [4], [5] have extended the idea to look at Gaussian waveforms which are an example of a completely smooth waveform. These works show clearly that waveforms exhibiting these characteristics are able to achieve an extremely high roll off. Considering the range of possible methods for modeling a
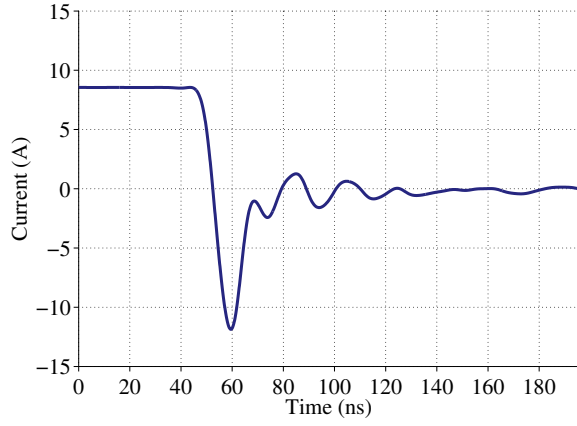
Fig. 5. Top switching device current waveform (I_D) for a hard switched SiC MOSFET based converter.
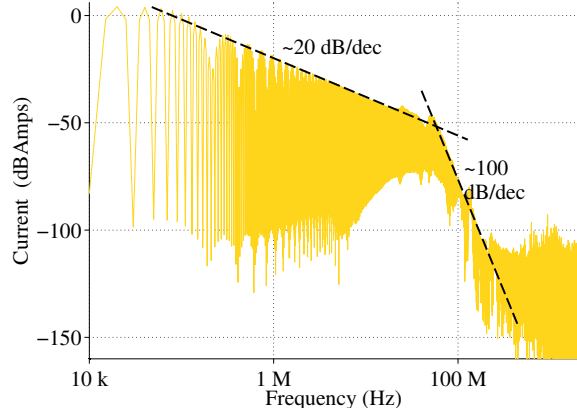

Fig. 6. Spectra of top switching device current waveform (I_D) for a hard switched SiC MOSFET based converter.

waveforms shape this presents it is clear that choosing a suitable one to analyze any particular, experimentally obtained, waveform could be very difficult.

III. APPLICATION TO REAL DATA

It has been established that data observed from a real application can often exhibit artifacts that are not expected when modeled with the basic trapezoidal waveform. An example of such data is presented in Figure 6 where a roll off of around 100 dB/dec is observed directly after a 20 dB/dec region. Given this spectrum and the time domain waveforms, it is not immediately clear which characteristics of the temporal waveform of Figure 5 lead to these spectral characteristics.

Given the understanding that smoother waveforms will lead to a faster roll off of spectral content, it would be expected to see some smoothness in the time domain waveform for this spectrum. By looking at the derivatives of the transitions and comparing them to the idealized ones shown previously in Figure 3 the smoothness of the waveform can be determined.

Figure 7 shows the rising edge of the experimentally obtained waveform and its first four derivatives. If this data were analyzed using the trapezoidal approximation it would not be possible to predict the high roll off seen in Figure 6. This approximation would also assume that the first derivative
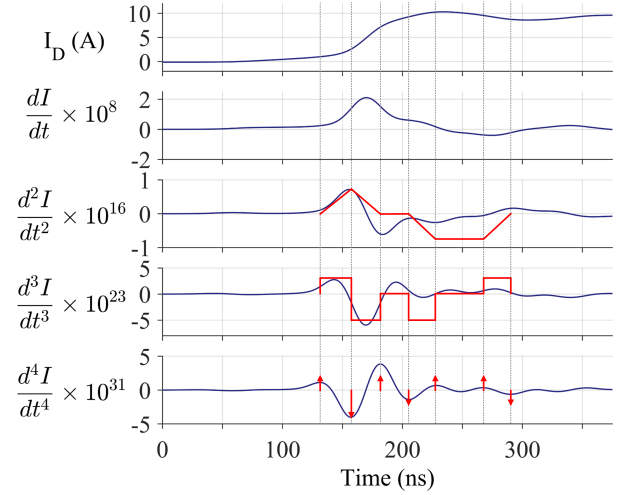

Fig. 7. Rising edge of the top switching device current waveform (I_D) in a real system with first four derivatives. A smoothing function has been applied to the data in order to suppress the noise.

of the temporal data would contain discontinuities - clearly this is not the case. Figure 7 shows that the data in fact is better represented by the 3rd or 4th order smoothed waveform. Considering the expression previously established linking the number of times a waveform can be differentiated and the maximum rate of roll off, the 100 dB/dec observed should indicate a 5th order system.

An important consideration when analyzing data taken from a real system is that the noise on the waveform will be massively amplified by differentiating [10]. This can make it practically impossible to discern any useful information from derivatives much past the first or second. As it is desirable to look at much higher derivatives of the data when analyzing it this issue needs to be resolved. Fortunately by applying filtering to the zero order derivative waveform to remove noise it is possible to improve the clarity of the higher derivatives of the waveform. To illustrate this the second derivative of the current waveform shown previously is shown in Figure 8 first without filtering, and below, with a function applied. As this is essential for ensuring that the information in higher derivatives is discernible it is used for all further successive derivative analyses in this work.

IV. INVESTIGATION OF PERFORMANCE VARIATION WITH CHANGING SWITCHING SPEED

Varying the switching speed clearly affects the performance of the converter. It is expected that the faster switching transients will reduce the switching losses while increasing the EMI. Changing the gate driver output resistance allows some control over the shape of the switching edge. As the importance of the shape of the switching waveforms and their derivatives has been established, it is clear that investigation of how these change when the gate resistor is varied will be of interest. Here an experimental system is discussed and a set of waveforms is analyzed.
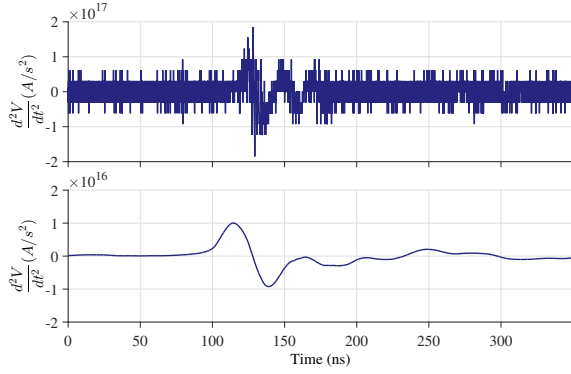
Fig. 8. Illustration of how the use of a smoothing function enables the clear analysis of further derivatives. The top plot is of the 2nd derivative of the current waveform with no smoothing applied. The bottom plot is with a 229 point rectangular smoothing function.
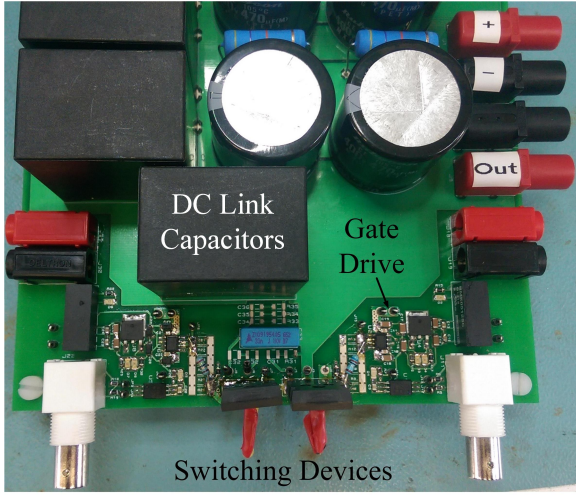

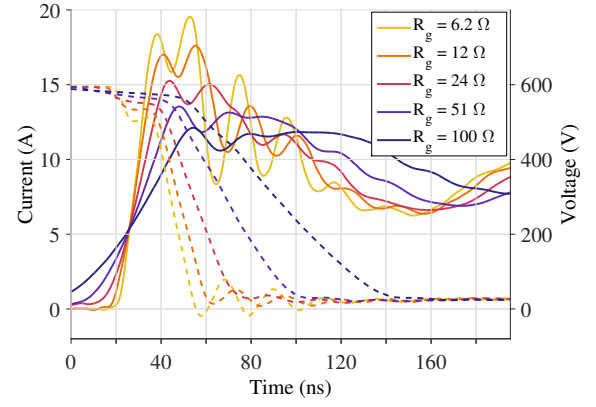Fig. 9. The experimental double pulse test circuit

Fig. 10. Experimental turn on current and voltage waveforms for varying gate resistance. Solid line: Current; Dashed line: Voltage

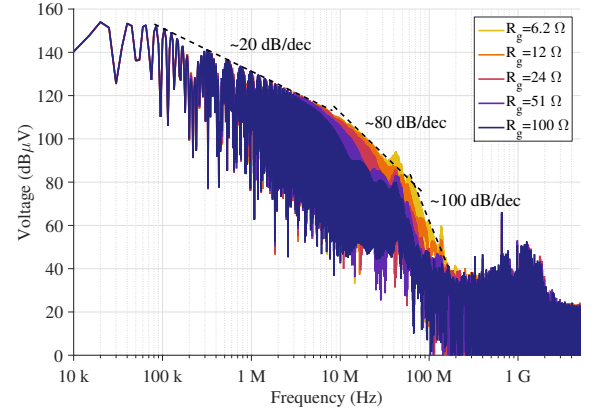Fig. 11. Spectra of the voltage waveforms from the experimental set up with varying gate resistance

A. Hardware set-up

A test circuit was assembled to perform both double pulse and continuous operation tests as shown in Figure 9. The circuit implements a single phase leg using Cree C2M0080120D SiC MOSFETs. Microchip TC4452VOA gate drive ICs drive the device gates using +20 V turn on and -5 V turn off supplies. Typically a DC supply voltage of 600 V was used as this is a common nominal value for rectified three phase mains. Altering the gate resistor allows the rate of change of voltage across the switching device during switching to be varied as indicated in Table II.

TABLE II
TESTED GATE RESISTANCES AND RESULTING dV/dt

Rg (Ω)	dV/dt ($kV/\mu s$)
100	4.9
51	8.4
24	15.6
12	23.7
6.2	29.8

B. Experimental test results

Experimental data was gathered from the test circuit over a range of gate resistance values. In order to produce reliable frequency domain results with the DFT the system was run continuously with the maximum possible capture window used on the oscilloscope while retaining the maximum sampling frequency.

The top switching device I_D and V_{DS} during turn on are shown in Figure 10, illustrating clearly that the overshoot and ringing increase significantly as the gate resistance is reduced. Figure 11 shows the results of taking the DFT of several cycles of the voltage waveforms seen in Figure 10. The largest difference between the envelopes is seen in the high frequency region of 5 MHz to 100 MHz after the first break-point. The spike in each of the waveforms at around 40 MHz can clearly be attributed to the ringing after switching.

C. Identification of ringing mechanism

In addition to the contributions of the fundamental characteristics of the switching waveform there are also parasitic effects that will contribute significantly to the spectrum. In particular, the overshoot and ringing on a waveform, which will add additional spectral content at well defined frequencies. Figure 5 clearly shows that the current waveform for this hard

switched converter overshoots the nominal value at turn on as well as oscillating at two distinct frequencies.

A thorough analysis of how ringing influences the spectral envelope of a waveform is presented in [8] where it is shown that overshoot can simply be considered as a special case of ringing with a very high damping factor. Ringing or overshoot on a waveform will have the effect of multiplying the expansion coefficients by a bandpass function - this produces a spike in the envelope and will be a problem for designers trying to work close to a given acceptable EMI limit.

During turn on of the top switching device a resonant network is formed from parasitic elements in the circuit. The characteristics of this network will be dominated by the influence of the lower device C_{oss}, the DC-link inductance and the load parasitics. There will also be an interaction between the parasitics in the converter and those of the load.

In order to calculate the frequency of resonance of a parallel CL network both the inductance and the capacitance are required. The capacitance in this case is simply taken from the device data-sheet (80 pF). The DC-link inductance is calculated from the droop in the voltage observed across the switching devices at the beginning of switching and the rate of change of current during this period. To demonstrate that using these values of components gives a reasonable approximation of the ringing frequency, and hence the position of an artifact on the spectra, they were measured and compared to the observed ringing frequency. Figure 12 shows a comparison of how the measured ringing frequency and the ringing frequency calculated through this method compare. It is seen that although the measured and the estimated frequencies are similar in magnitude there is still a significant discrepancy.

The transfer function of the resonant network formed by a capacitance and an inductance will have a classic bandpass shape. When a voltage profile is applied to this network the spectral envelope of the resulting current will be the multiplication of this bandpass filter and the spectra of the input waveform. This leads to the spectra observed in Figure 14. The peak of the resultant spectra can then be suppressed through a number of different methods; the transfer function can be modified by manipulating the parasitic values; additional components can be added to form additional filtering; or the excitation can be modified. Figure 4 shows that smoothing the waveform edges can reduce the amplitude of the spectral envelope, this would then lead to a reduction in the amplitude of the ringing.

A simulation was carried out in which the parasitic elements of the circuit discussed were excited with waveforms of varying smoothness as shown in Figure 3. The resulting current was recorded and the peak to peak amplitude of the ringing plotted in Figure 13. This figure shows that for any given switching speed tested, that the smoother the waveform (corresponding to higher values of D), the lower the amplitude of the ringing.

The results here show that it is possible, at increased switching speeds, to predict with some accuracy the frequency at which ringing is likely to occur with only very simple
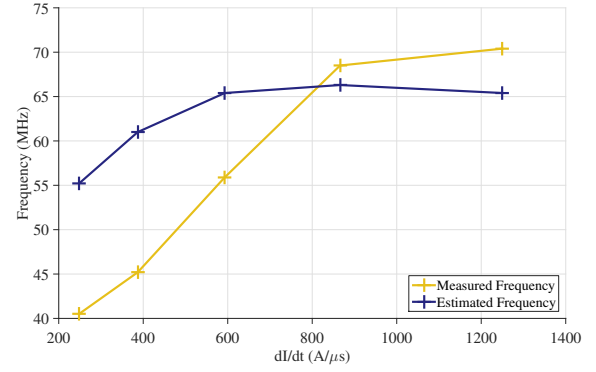

Fig. 12. Comparison of the observed ringing frequency and the calculated ringing frequency at turn on with differing switching speeds.
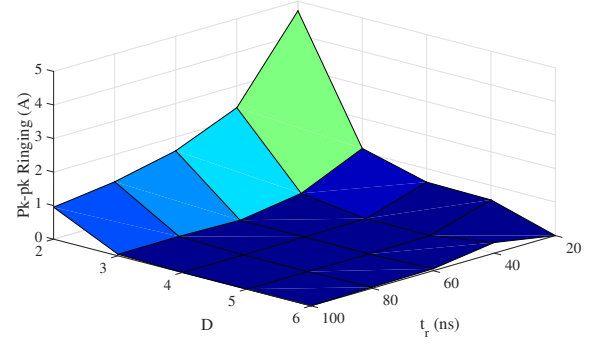

Fig. 13. Variation of ringing amplitude on the current waveform at turn on for varying rise time and excitation smoothness
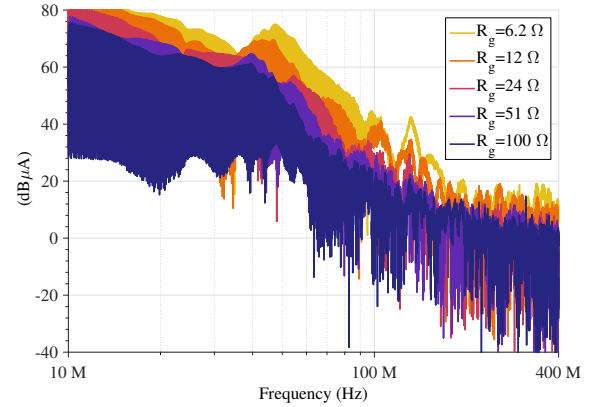

Fig. 14. Spectra of current waveforms with varying gate resistance

knowledge of the system. In addition to this it is clear that the ringing could be reduced by smoothing the voltage waveform applied to parasitic networks, leading to better performance under the influence of parasitics. The extension of these simulated results to an experimental demonstration is beyond the scope of the work presented here.

D. Multi-derivative analysis

The experimental results obtained can now be analyzed using the method of successive differentials discussed previously. To show the differing characteristics most clearly the two most extreme cases will be compared, the case where $R_g = 100 \ \Omega$ and that where $R_g = 6.2 \ \Omega$. Both the turn-on and turn-off
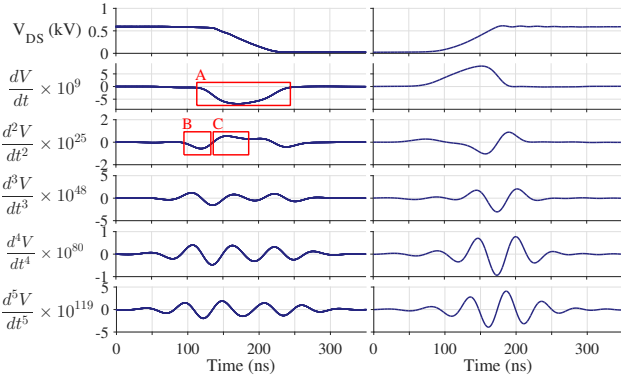
Fig. 15. V_{DS} and its first five derivatives for the top switching device with $R_g = 100\ \Omega$. Left: turn on. Right: turn off.

Fig. 16. V_{DS} and its first five derivatives for the top switching device with $R_g = 6.2\ \Omega$. Left: turn on. Right: turn off

of the device will be considered as the characteristics of each can vary significantly. Figure 11 shows that the roll off for each of the cases investigated occurs at a similar rate, and from a similar break-point. Given this it would be expected that the waveforms will have similar characteristic shapes. In the 5-100 MHz region of Figure 11 the amplitude of each of the spectra is significantly different in amplitude. This indicates that the amplitude of the derivatives of the temporal waveform will likely increase with the increase in amplitude of the spectral envelope.

In Figure 15 the transition time of the voltage waveform is around 100 ns and the first derivative has a very smooth shape (A). This would be expected as the roll off of the spectra is around 100 dB/dec indicating a set of derivatives similar to the 5th order case. Considering the second derivative of the waveform it would be expected this would be similar in characteristic to the second derivative of the 4th order smoothed waveform presented in Figure 2 but with smoothed corners. The initial negative going portion of the turn on waveform is as expected (B), however following this there is a positive going portion (C) where a zero portion would be expected. This shows that the first derivative immediately begins its rise after reaching it's peak negative value. The following derivatives become increasingly difficult to compare to the example waveforms.

In the case of $R_g = 6.2\ \Omega$ shown in Figure 16 the transition time of the voltage is only 40 ns. As for the higher gate resistance case the expectation will be to observe derivatives that have characteristics of the 5th order example. Again the first derivative is close to what would be predicted from the theory (E), however the second derivative presents some problems - this is because following the expected negative pulse (F) and positive pulse (G) there is then another negative pulse (H). Looking at the original signal it can be seen that this deviation form the prediction is due to ringing on the waveform (D).

Comparing the turn-off waveforms to the turn-on waveforms, it can be seen that the derivatives remain similar in amplitude for any particular value of gate resistance. This is because the transition time of the voltage waveform is
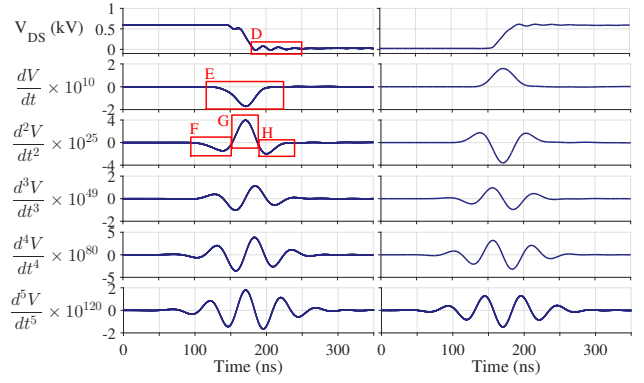
similar for both turn-on and turn-off. The characteristics in each further derivative are also similar to those during turn-on, indicating that either switching edge could be considered with this analysis to form a picture of the overall behavior.

From this analysis it is clear that it is possible to make some predictions about the roll-off of the spectrum of a waveform simply by looking at the derivatives of a single switching edge. However, it is also shown that ringing on the waveform and even relatively small deviations from the ideal cases renders this method difficult to use to get accurate information. Perhaps the greatest use of this tool is to look at the first and second derivative to quickly establish the likely rate of roll-off at high frequencies.

E. EMI analysis

When considering the spectral characteristics of power converter waveforms it is useful to be able to quantify their severity with a single number to aid comparison, as well as identify particular characteristics in more detail. This has motivated the work of [11], in which a metric is developed which quantifies the EMI performance of a design. This metric fits the design of a filter to the required attenuation for a given spectra, the comparison metric is then the break-point of that filter. This metric is applied to the waveforms presented in this work with the EN5022 standard used as the reference. The spectra of the V_{DS} waveform for the $R_g = 100\ \Omega$ case is shown in Figure 17, here the spectra of the voltage waveform is far above the standard as the completely unfiltered waveform is being considered.

As this metric assumes that an ideal filter is being used and the data considered here are over the specified limit in the lower frequencies the performance difference indicated is only a reflection of the spectral amplitude at the lower limit of the specification. The high frequency characteristics are not taken into account as they are obscured by the lower frequency characteristics. This limitation motivates considering in further detail the characteristics of the spectral envelope.

From traditional techniques it is simple to calculate that with increased switching speed the spectral envelope will be increased [1]. The maximum switching speed for the waveform is the peak of its first derivative which indicates
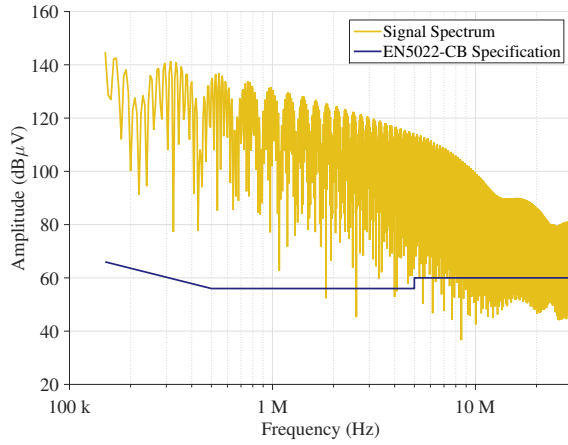
Fig. 17. Demonstration of the calculation of the performance metric described in [11] using the spectra of the voltage waveform where $R_g = 100\ \Omega$. Here the break-point for a first order filter is $17.2\ Hz$
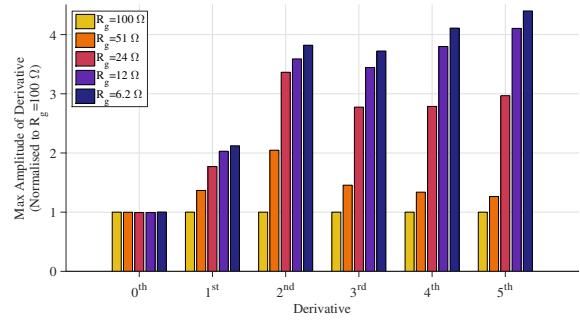

Fig. 18. Peak amplitude of each derivative of the waveform for various cases of R_g. Each set has been normalized to the $R_g = 100\ \Omega$ case

that higher values of the first derivative of a waveform will indicate higher levels of EMI.

Equations (5) and (6) show the break-frequencies for the trapezoidal waveform [1] and Equations (7) to (9) show those for the S-shaped waveform [6]. The break frequencies give the points at which the spectral envelope of the waveform transitions from one roll-off rate to a steeper one. The lower these frequencies are, the lower the high frequency components of the spectral envelope of a waveform will be. For each waveform, the higher the break-point considered, the more of the higher derivatives are introduced. For some an increase in the amplitude of the derivative will decrease the break-frequency such as in Equation (9) whereas for others it will increase the break-frequency, such as in Equation (8). For the trapezoidal case: For the S-shaped case:

$$f_{c1} = \frac{1}{\pi\tau} \qquad (5) \qquad\qquad f_{c1} = \frac{1}{\pi\tau} \qquad (7)$$

$$f_{c1} = \frac{1}{\pi\tau_r} \qquad (6) \qquad f_{c2} = \frac{1}{\pi(\tau_r - \tau_{r(f'(t))})} \qquad (8)$$

$$f_{c3} = \frac{1}{\pi\tau_{r(f'(t))}} \qquad (9)$$

To explore this the relative maximum amplitude of each of the derivatives of the V_{DS} waveform are shown in Figure 18. The values within each derivative are normalized to the slowest switching speed ($R_g = 100\ \Omega$) to aid comparison. It is shown in the figure that the zero order derivative has close to equal amplitude for all of the cases of switching speed, this is expected as this will be determined by the DC-link voltage with deviations indicating where there is overshoot. In the following derivatives the difference between the low and high speed switching gets increasingly large - in the case of the first derivative the fastest case has a value just twice that of the slowest case whereas in the fifth derivative the fastest switching speed has an amplitude more than four times that of the slowest case.

The use of the successive derivative analysis to analyze the switching waveforms for this converter is able to reveal characteristics of the spectra that are not easily quantified through the use of the existing metric. The ability to compare the spectral performance of a converters waveforms under various operating conditions with this technique helps to identify where in a waveform significant noise is being generated.

F. Comparison of performance metrics

Through this work several methods of assessing the performance of a power converter have been considered. To evaluate the overall performance of a converter an understanding of performance metrics of different aspects of the converter will be required. One of the most common metrics used is the switching loss as this is easy to calculate from measurements. Here this will be used as a metric to compare the performance of the switching edges. In addition to the switching loss metric, it is also desirable to be able to compare the EMI performance of different switching edges. The first metric that can be used for this is the one previously explored and described in [11]. The break-frequency of the filter for each of the switching edges can be compared. As discussed earlier, the peak amplitude of each of the derivatives of a waveform can also be used as an indicator of the performance at various frequencies. In order to establish the feasibility of using this as a performance metric the maximum amplitude of the first derivative is recorded for each of the switching speeds.

Each of these metrics is plotted in Figure 19 against switching speed. It is desirable for the switching loss to be as low as possible, the amplitude of the first derivative to be as low as possible and for the filter break-point of the EMI metric to be as high as possible. Interestingly at the lower switching speeds the rate at which any of the metrics changes is quite fast; the switching losses are improving quickly and the EMI performance is reduced quickly. At higher switching speeds the performance of both the switching losses and the EMI begins to plateau. It is interesting to note that the maximum value of the first derivative should be close to the switching speed, which on this graph should produce a straight line. However, as the waveform shapes are not ideal, the actual switching speed and the peak rate of change can actually deviate significantly. This is particularly apparent for the slowest switching speed case considered here where the
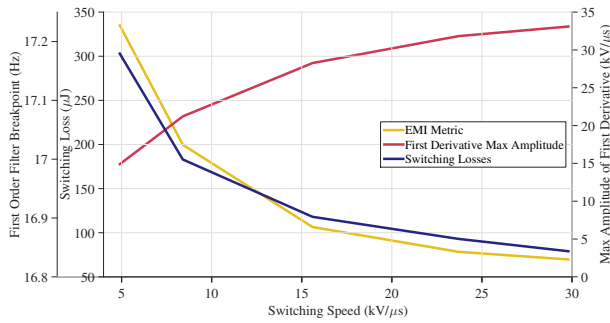
Fig. 19. Comparison of the variation of the different performance metrics with varying switching speeds

maximum rate of change of voltage is actually around three times the average switching speed measured.

The consideration of each of these metrics highlights the importance of the switching-loss to EMI trade-off that must be reached in the design of a converter's switching waveforms. In particular it demonstrates that the information in the derivatives of a switching waveform can inform a design by quickly identifying the temporal source of high frequency characteristics. It is clear that the particulars of the shape of a waveform will significantly impact the EMI performance without necessarily resulting in a faster switching speed.

V. Conclusion

In this work it has been shown that it is possible to determine the characteristics that lead to a particular spectral shape by considering the smoothness of a given temporal waveform. By taking successive differentials of the temporal data and applying a suitable smoothing function the temporal data can be compared to the idealized cases to determine where smoother aspects of the waveform are taking place.

It is also clear from this work, that the analysis presented can be used to design waveforms as well as analyze them. It is shown through analysis and simulation that the practical realization of smoothed waveforms of this type could not only lead to improvements in the EMI performance of the system, but also improve the temporal performance under the influence of parasitic elements. Given an understanding of how the smoothness of a waveform can reduce the high frequency spectral components, adequate control could lead to improved converter performance as demonstrated in [4], [5], [12]–[14].

A critical consideration for power converter performance is the switching-loss/EMI tradeoff. It has been considered here how the methods discussed can help to inform such a tradeoff and the need for more advanced metrics to asses power converter waveforms has been highlighted. To complement these techniques methods for analyzing power electronics waveforms that utilize wavelets such as the works of [15], [16] will be compared with the techniques discussed here.

Future work will compare wavelets with the techniques presented here. A method for controlling the smoothness in the experimental system will also be developed as well as metrics for the quantification of both the EMI and smoothness that help to solve the trade-off between EMI and losses.

References

[1] A. Nagel and R. De Doncker, "Analytical approximations of interference spectra generated by power converters," in *Industry Applications Conference, 1997. Thirty-Second IAS Annual Meeting, IAS '97., Conference Record of the 1997 IEEE*, vol. 2, Oct 1997, pp. 1564–1570 vol.2.

[2] F. Costa and D. Magnon, "Graphical analysis of the spectra of emi sources in power electronics," *Power Electronics, IEEE Transactions on*, vol. 20, no. 6, pp. 1491–1498, Nov 2005.

[3] J. Balcells, D. González, M. Lamich, and D. Bedford, "Emi generation models for switched mode power supplies," *Fifth European space power conference (ESPC)*, vol. 2, pp. 421–426, 1998. [Online]. Available: http://articles.adsabs.harvard.edu/

[4] X. Yang, Y. Yuan, X. Zhang, and P. Palmer, "Shaping high-power igbt switching transitions by active voltage control for reduced emi generation," in *Industry Applications, IEEE Transactions on*, vol. 51, no. 2, IEEE. IEEE, March 2015, pp. 1669 – 1677.

[5] N. Patin and M. L. Vifials, "Toward an optimal heisenberg's closed-loop gate drive for power mosfets," in *IECON 2012 - 38th Annual Conference on IEEE Industrial Electronics Society*. IEEE, October 2012, pp. 828 – 833.

[6] N. Oswald, B. H. Stark, D. Holliday, C. Hargis, and B. Drury, "Analysis of shaped pulse transitions in power electronic switching waveforms for reduced emi generation," *IEEE Transactions on Industry Applications*, vol. 47, no. 5, pp. 2154–2165, 2011.

[7] R. H. Bartels, J. C. Bealty, and J. C. Beatty, *An Introduction to Splines for Use in Computer Graphics and Geometric Modeling*. Morgan Kaufmann Publishers Inc., 1995.

[8] R. P. Clayton, *Introduction to Electromagnetic Compatibility*, 2nd ed. Wiley, 2006.

[9] N. F. Oswald, "Towards an improved trade- off between switching losses and radiated emi generation in hard-switched power converters," PhD, University of Bristol, 2012.

[10] J. Cullum, "Numerical differentiation and regularization," *SIAM Journal on Numerical Analysis*, vol. 8, no. 2, pp. 254–265, 1971. [Online]. Available: http://dx.doi.org/10.1137/0708026

[11] K. Mainali, R. Oruganti, K. Viswanathan, and S. P. Ng, "A metric for evaluating the emi spectra of power converters," *IEEE Transactions on Power Electronics*, vol. 23, no. 4, pp. 2075–2081, July 2008.

[12] F. Reby, R. Bausiere, B. Sohier, and F. Costa, "Reduction of radiated and conducted emissions in power electronic circuits by the continuous derivative control method (cdcm)," in *Power Electronics and Variable Speed Drives, 1998. Seventh International Conference on (Conf. Publ. No. 456)*, Sep 1998, pp. 158–162.

[13] M. Blank, T. Gluck, A. Kugi, and H.-P. Kreuter, "Digital slew rate and s-shape control for smart power switches to reduce emi generation," *Power Electronics, IEEE Transactions on*, vol. 30, no. 9, pp. 5170–5180, Sept 2015.

[14] X. Yang and P. Palmer, "Shaping pulse transitions by active voltage control for reduced emi generation," in *Energy Conversion Congress and Exposition (ECCE), 2013 IEEE*, Sept 2013, pp. 1682–1687.

[15] E. Wernekinck, H. Valenzuela, and I. Anfossi, "On the analysis of power electronics circuits waveforms with wavelets," in *Power Conversion Conference, 1993. Yokohama 1993., Conference Record of the*, April 1993, pp. 544–549.

[16] K. Serguei and B. Serguei, "A wavelet method for signal analyses of the power electronics circuits," in *Science and Technology, 2003. Proceedings KORUS 2003. The 7th Korea-Russia International Symposium on*, vol. 2, July 2003, pp. 129–131 vol.2.